Nuclear Instruments and Methods in Physics Research A317 (1992) 135–142
North-Holland

NUCLEAR
INSTRUMENTS
& METHODS
IN PHYSICS
RESEARCH
Section A

A large acceptance threshold Cherenkov counter for Experiment 760 at Fermilab

C. Biino, G. Borreani, A. Ceccucci, R. Cester, G. Dughera, G. Giraudo, F. Marchetto, E. Menichetti, A. Migliori, R. Mussa, S. Palestini, N. Pastrone, L. Pesando and G. Rinaudo
I.N.F.N. and University of Torino, 10125 Torino, Italy

M.A. Mandelkern
University of California, Irvine, CA 92717, USA

Received 16 December 1991

A threshold gas Cherenkov counter is used in Fermilab Experiment 760 to tag electrons in the detection of charmonium states. Mechanical structures and mirrors were built with carbon-fiber–epoxy composites, resulting in a light weight detector covering 2π in azimuthal angle. The counter is operated at atmospheric pressure with different gases, CO_2 and Freon 13, respectively in the two cells at small and large polar angles, to maximize pion rejection. Design considerations, construction details, and performance of the counter are described.

1. Introduction

Experiment 760 at the Fermi National Accelerator Laboratory studies charmonium states formed in the annihilation of an antiproton beam, circulating in the $\bar{p}$ Accumulator, on the protons of a molecular hydrogen beam (gas jet) [1]. Part of the experiment is devoted to studying reactions such as:

$$\bar{p}p \to (c\bar{c}) \to J/\psi + \text{anything} \qquad J/\psi \to e^+e^-. \quad (1)$$

A threshold gas Cherenkov counter was built as part of the charged particle trigger system to select electrons out of a large background of hadrons.

The detector was designed to maximize the solid angle acceptance in the forward hemisphere within the available region, a cylindrical shell around the beam line with an inner radius of 17 cm and an outer radius of 59 cm. The counter is subdivided into two separate gas tight cells, that cover the polar angle (θ) regions from 15° to 38° and from 38° to 70° [#1], respectively. Each cell is optically segmented in eight sections, covering 45° in azimuth (ϕ) per section.

A light collection system of efficient and simple design was possible since the object size, determined by the particles source size and by the Cherenkov light aperture cone, is relatively small. To minimize weight and the amount of material traversed by the particles, the mechanical structures and mirrors were built using carbon-fiber–epoxy composites.

The counter is operated at atmospheric pressure and room temperature, using different gases in the two cells, to optimize both the electron detection efficiency and e/π separation.

In this paper we discuss the design and the performance of the counter, as determined from the study of about 5000 J/ψ, collected in the first E760 data taking period, from reaction:

$$\bar{p}p \to J/\psi \to e^+e^-. \quad (2)$$

The measured photoelectron yield is also compared to the yield expected from a Monte Carlo simulation.

2. General characteristics and design

The characteristics of the counter are summarized in table 1.

Henceforth we shall refer to the cell crossed by particles emitted from the interaction region with polar angle in the range $15° < \theta < 38°$ as *small angle cell* and

[#1] The maximum angle allowed by space occupation of the jet target complex is $\theta_{max} = 70°$. The choice of θ_{min} is then dictated by the correlation in the emission angle of the two electrons in a reaction of type (1). For instance in the process: $\bar{p}p \to \chi \to J/\psi + \gamma$ $J/\psi \to e^+e^-$, 88% of the events having $\theta_{e_1} < 70°$, have $\theta_{e_2} > 15°$. Thus the choice of $\theta_{min} = 15°$ appears to be reasonable; to lower θ_{min} to, say, 10°, would have posed serious problems of optics design and gas choice, while adding only 10% to the acceptance.

Table 1
Characteristics of the counter

	Angular aperture $15° < \theta < 38°$	Angular aperture $38° < \theta < 70°$
ϕ segmentation	45° ×8	45° ×8
Gas (atm. pressure)	CO_2	Freon 13 (CF_3Cl)
Refractive index	1.000410	1.000720
θ_c	1.64°	2.17°
π threshold [GeV/c]	4.873	3.677
Mirrors	Ellipsoidal	Spherical
Dimensions [mm]	half axes: $a = 900$, $b = c = 450$	Radius = 548
Retro-reflecting	–	Plane aluminized glass
Photomultipliers	Hamamatsu R1332Q	Hamamatsu R1332Q
Number/diameter [in.]	8/2	8/2
Radiator length [cm]	98–66	34–39
Light collection efficiency	1.0–0.75	0.95–1.0

to the cell traversed by particles with $38° < \theta < 70°$ as *large angle cell* (fig. 1a).

2.1. Radiator

The counter is operated at atmospheric pressure, with CO_2 in the small angle cell and Freon 13 in the large angle cell.

Notice that the useful radiation length, in the small angle cell, is a rapidly decreasing function of the polar angle; the gas tight partition between the two regions was positioned at $\theta = 38°$ where the calculated photon yield would be about the same on either side of the boundary.

A convenient choice of the refractive indices resulted from the following considerations:

1) Ideally we would like to reject completely the hadron component. This criterion is nearly met if we choose the gas Cherenkov threshold $\beta_{th} = 1/n$ above the maximum value for the velocity of pions emitted in reaction $\bar{p}p \to \pi^+\pi^-$. Since the particle velocity in a two body reaction increases with decreasing polar angle, this criterion imposes the use of a radiator with the lowest index of refraction at small angles, allowing the use of a gas with higher refractive index at larger angles.

2) In a cylindrical geometry, the path length of electrons within the radiator decreases with increasing polar angle. It is therefore important to use in the large angle cell a gas with the highest possible refractive index to maximize the yield of Cherenkov light.

Additional criteria, which determined the final choice, were the use of comparatively low light absorbing, non explosive gases. This last point was of particular importance to reduce safety hazards in the Antiproton Accumulator tunnel.

We notice that π's emitted from the reaction $\bar{p}p \to \pi^+\pi^-$ at 15° cross the Cherenkov threshold ($\beta = \beta_{th}$) in CO_2 when the center of mass energy is $\sqrt{s} \simeq 3.4$ GeV. Similarly, π's emitted at 38°, in Freon 13, cross the Cherenkov threshold when $\sqrt{s} \simeq 5.8$ GeV.

2.2. Optical system

In the source–detector configuration of E760, particles from $\bar{p}p$ collisions originate from a point-like source ($2.5 \times 2.5 \times 8$ mm^3); thus the associated Cherenkov light can be focussed by converging mirrors into a relatively small image at the photomultiplier (PM) window. To optimize light collection efficiency two schemes are used in the two ranges of polar angles.

In the large angle cell each of the 8 sectors in ϕ is equipped with a focussing spherical mirror and a plane mirror to reflect the light onto a PM placed in the proper alcove of the counter's back wall (fig. 1a). The alcoves partly shadow the ϕ acceptance for $\theta > 59°$ reducing it from 2π to about $2\pi(1 - 0.067)$ for $54° < \theta < 59°$ and to $2\pi(1 - 0.53)$ for $59° < \theta < 70°$. Mirrors are suspended from the support structure with 1 mm diameter stainless steel wires.

The small angle cell contains 8 ellipsoidal mirrors, with common focus in the center of the interaction region, and rotational axes tilted 8.5° relative to the beam line and equally spaced in ϕ (45°). With this geometry the second foci lay at the vertices of a regular octagon, where the PM windows are placed (fig. 1b). Light coming from an annular virtual source centered on the interaction region is directly focused onto the PM windows. Each of the mirrors is supported by 3 spherical couplings. All PMs are Hamamatsu R1332Q (2 in. diameter and fused silica window).

2.3. Mirrors

The small plane mirrors are conventional 0.8 mm thick aluminized glass mirrors. The spherical and ellipsoidal mirrors were built with a carbon-fiber–epoxy composite (thickness 4 mm, corresponding to 0.65

g/cm^2): this choice, while adequate to our purposes as regards precision and reflectivity, has the advantage, over glass, of having low atomic number and weight. The cheap slumping technique used to produce glass mirrors would not has been practicable to produce the wide aperture ellipsoidal mirrors.

The mirrors were manufactured with a specially devised technique [2] that makes use of a convex cast iron mould and a concave carbon-fiber counter-mould. The metal mould was machined [under numerical control] to a precision of 0.01 mm and then polished to reach a roughness of 0.1, to avoid imperfections of its surface being transferred into the mirror surface. Carbon-fiber panels were laid upon the counter-mould together with layers of 824LST epoxy resin. The cast iron mould, spread with a thin layer of Gelcoat 4013 Rezolin (SAI ALCAN) and a thin layer of a mixture of epoxy and glass microspheres 3 μm in diameter (3M) was pressed from above at 30 bar until polimerization had taken place. The panels were then stabilized by heating and keeping them at 90°C, under the same pressure, for one hour. To produce an acceptable

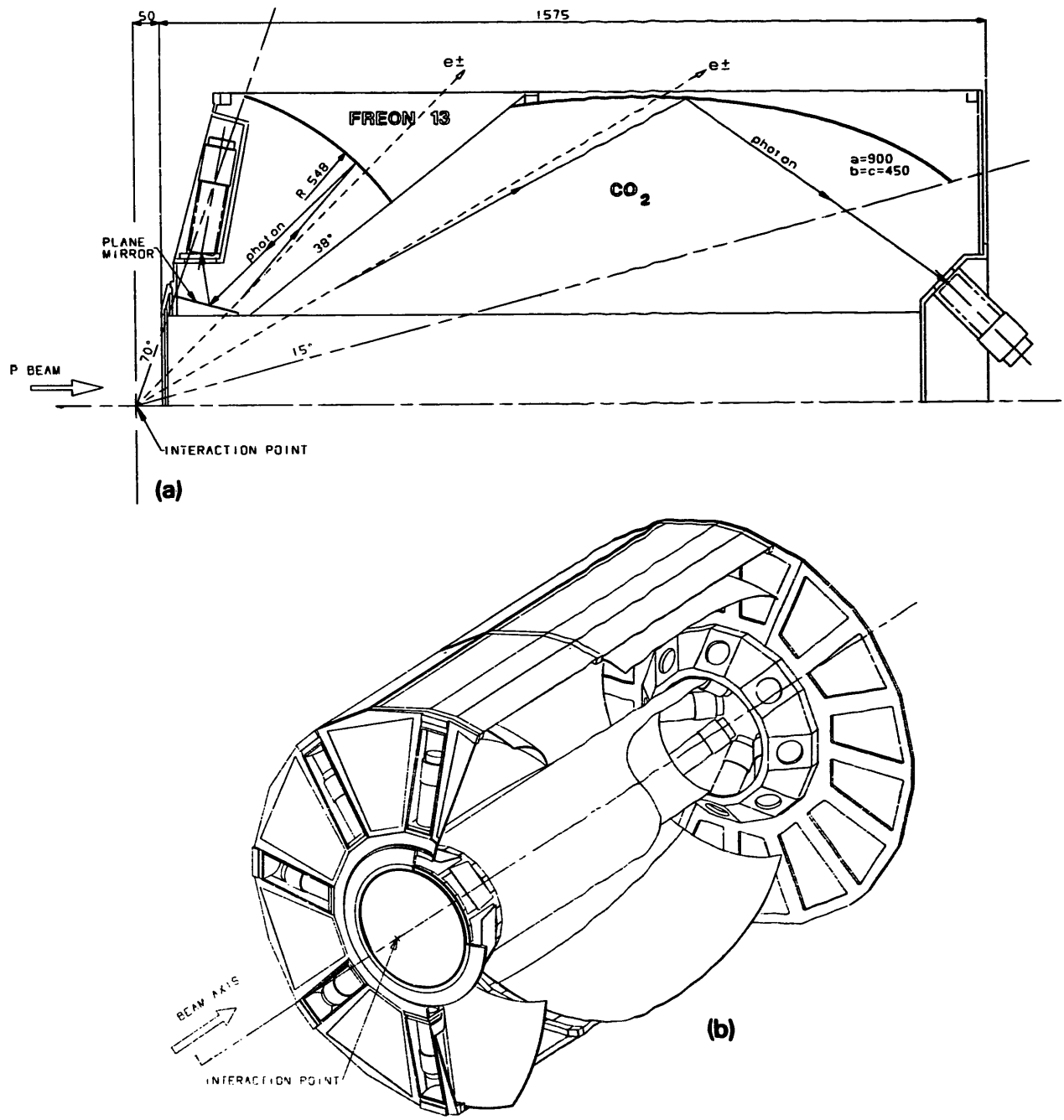

Fig. 1. Two views of the counter: (a) a transverse view showing the optical system; (b) an isometric view of the detector.

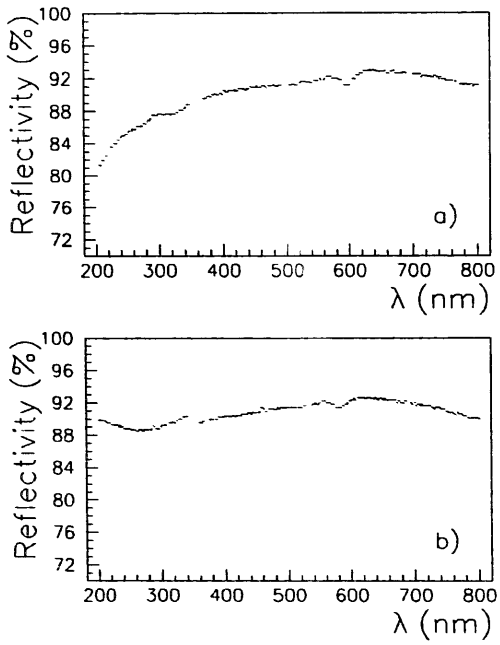

Fig. 2. Reflectance vs wavelength (unpolarized light, 30° incidence): (a) carbon-fiber with lacquered mirror, (b) glass mirror.

mirror, the panels had to be lacquered before aluminum deposition by dip painting with Neogene SV755 paint (undiluted) (Neogene Paints, London). After this treatment, Al and MgF_2 deposition under vacuum did not present special problems, except that a longer pumping time (24 h) was needed in order to obtain the necessary vacuum of $< 10^{-6}$ Torr.

Fig. 2a shows typical reflectances as a function of wavelength; for comparison fig. 2b shows the same for a typical plane glass mirror used in our counter.

2.4. Mechanics

The counter body, shown in fig. 1b, is bound by two surfaces coaxial with the $\bar{p}$ beam line, connected upstream by a truncated pyramid of semiaperture $\theta = 70°$ and downstream by a plane vertical wall. The outer shell, an irregular prism with 24 faces, is made of carbon-fiber–epoxy composite panels 1 mm thick glued onto a glass–reinforced-polyester frame that embodies the threaded holes for mirror support and adjustment. The end walls are bolted onto the prism and are light weight frames of the same polyester, to which 8 and 32 (back and front, respectively) aluminum windows 0.3 mm thick are fixed. These windows are used to permit access to the mirror supports while assembling the optical system and also to let a beam of light enter the counter during optics alignment. The photomultiplier supports are made of epoxy resin ST100VB (Vagnone Boeri, Torino) [#2]; as seen in fig. 1b, 8 photomultipliers are fit into 8 alcoves that are part of the back wall, while the remaining 8 are fit onto a unique frame bolted to the front wall. The inner cylinder is made of 0.3 mm thick carbon-fiber–epoxy and acts as a thin entrance window to the incoming particles. The gas tight pyramidal (24 faces) septum at $\theta = 38°$ is made of 0.3 mm thick aluminum foil.

The extensive use of plastic and carbon-fiber materials was motivated by physical mechanical requirements such as low Z, light weight, high strength and rigidity. In particular, from the mechanical point of view, light weight and rigidity were essential to allow support of the counter by four bolts at its upstream end only, thus leaving free space for the downstream detectors. The counter total weight is about 80 kg.

All the internal surfaces were blackened to absorb light not directly focussed by the mirrors on the PMs.

2.5. Optical alignment

To center the optical system, we used a laser beam impinging on a plane, white surface, simulating by diffusion an isotropic light source at the nominal position of the interaction point. The partition between the two cells was positioned to define a cone with its vertex on the interaction point, the axis on the beam line and a half angle of 38°.

The choice of using the nominal interaction region to align mirrors and position the gas tight partition generated a rigid constraint when positioning the counter within the apparatus. The spherical mirrors' optics is the most sensitive to the position of the counter. During the first test in 1988, due to mechanical interference, the counter was placed 2.5 cm downstream from the nominal position, reducing the light collection efficiency in the large angle cell to about

[#2] The support is manufactured by pouring the two component resin into a mould at room temperature.

Table 2
Simulation results: cell at $15° < \theta < 38°$

θ	15°–18°	18°–21°	21–24°	24°–27°	27°–30°	30°–34°	34°–38°
ϵ_{geom}	1.0	1.0	1.0	1.0	1.0	0.94	0.75
L_{rad} [cm]	93.1	94.6	92.3	87.7	81.7	74.2	65.6
$\Delta\alpha_{inc}$	24°–66°	6°–48°	0°–36°	0°–30°	0°–30°	0°–30°	12°–36°
$\langle n_{pe} \rangle$	11.4	11.1	10.7	10.3	9.6	8.1	5.8

Table 3
Simulation results: cell at $38° < \theta < 70°$

θ	38°–42°	42°–46°	46°–50°	50°–54°	54°–59°	59°–70°
ϵ_{geom}	0.95	0.98	0.99	1.0	1.0	1.0
L_{rad} [cm]	34.7	36.0	37.0	37.9	38.5	38.8
$\Delta\alpha_{inc}$	30°–48°	24°–42°	18°–36°	18°–36°	12°–36°	6°–30°
$\langle n_{pe}\rangle$	6.7	7.2	7.5	7.7	7.9	7.9

50%. Moreover, in this situation, the partition shadowed polar angles between 35° and 38°, dramatically reducing the efficiency in this region.

During the physics run of 1990 the counter was positioned about 1 cm downstream from the nominal position. The main effect was then a loss of electron identification at $36° < \theta < 38°$ due to shadowing from the partition.

3. Calculated photoelectron yield

3.1. Light collection efficiency

For both optical schemes (spherical and ellipsoidal mirrors) a ray tracing program was used to determine, as a function of θ, the geometrical collection efficiency of the 2 in. PMs and the useful radiator length (L_{rad}).

The results are summarized in tables 2 and 3, where are also listed the range of the photon incidence angle on the PM window (α_{inc}) [#3] and the PM photoelectron yield, calculated as explained in the next subsection.

As can be seen, the geometrical collection efficiency is sizably reduced between $\theta = 30°$ and $\theta = 42°$; the effect comes from the image size exceeding the sensitive area of the photocathode of our 2 in. PM. This would have made the choice of a 3 in. tube more suitable, however no commercial 3 in. PM met our requirements, i.e.:

1) High quantum efficiency down to 200 nm wavelength.

2) Good one photon resolution (needed to reject charged pions with an associated δ ray).

3) Fast rise time (2–3 ns) for optimum time definition of the electron trigger.

The optical system data, input to the tracing program, are given in table 1. Electrons were generated for each angular interval and followed through the counter. The beginning and end point of the useful trajectory in the radiator were determined. A number of photons per electron was then randomly generated, with the Cherenkov angle appropriate to $\beta = 1$ particles, along the trajectory inside the radiator volume. Each of them was followed through the optical system to the PM window. The fraction of photons whose impact distance from the center of the PM window was less than 2.16 cm (useful radius of the photocathode) defined the geometrical light collection efficiency. Refractive indices of CO_2 and Freon 13 were respectively used in the small and large angle cells.

3.2. Photoelectron yield

In the calculation of the photoelectron yield a precise knowledge of the quantum efficiency of the PM cathode plays a crucial role. Unfortunately, quantum efficiency curves given by the manufacturer lead, in general, to discrepancies between the calculated and measured average number of photoelectrons. To overcome this problem we adopted a semiempirical method taking advantage of the experience gained in experiment R704 [3] with RCA C31000M photomultipliers, similar in design to the Hamamatsu R1332Q. After testing that the performances of the two types of photomultipliers were indeed quite similar we proceeded to calculate the photoelectron yield in the present situation from the experimental results of the R704 counter. We calculated the average number of photoelectrons $\langle n_{pe}\rangle$ as:

$$\langle n_{pe}\rangle = N_0 L_{rad} \sin^2\theta_c ,$$

where L_{rad} is the radiator length, θ_c is the Cherenkov angle and N_0 is the empirical parameter that incorporates the efficiencies of the optical systems (geometrical, reflectivity of mirrors, absorption in the gas) and the quantum efficiency of the photomultiplier. For the R704 counter we measured $N_0 = 131\ \text{cm}^{-1}$, with an average geometrical light collection efficiency of 0.92 [#4], here we used $N_0(\theta) = 131\ \epsilon_{geom}(\theta)/0.92\ \text{cm}^{-1}$ to account for the different geometrical efficiencies. We point out that this assumption leads to underestimate the number of photoelectrons at small azimuthal angles, since it does not take into account the fact that a smaller image samples the most sensitive area of the PM photocathode.

[#3] Measurements showed no sign of decrease of response for incident angles up to 65°.

[#4] Determined with Freon 13. A test with CO_2 in the R704 counter produced a comparable value of N_0.

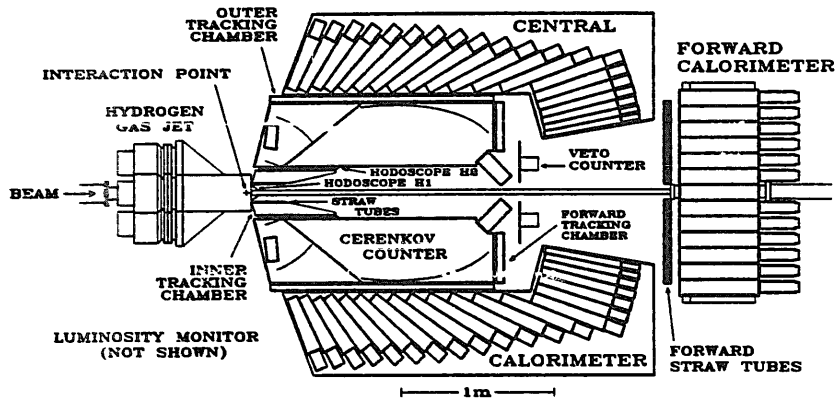

Fig. 3. Layout of the E760 detector.

4. Performance of the counter

With the study of a sample of about 10000 electrons from reaction (2), we determined the average number of photoelectrons measured in the counter as a function of θ and ϕ to be compared with the results of the simulation.

4.1. Event selection

A logic to select effectively all ($c\bar{c}$) resonances decaying either inclusively to a J/ψ or exclusively to e^+e^- was implemented at the fast trigger level.

The elements entering this trigger were (fig. 3): two layers of scintillator hodoscopes (H1 and H2), the Cherenkov counter and a lead glass calorimeter. An appropriate coincidence between H1 and H2 defined a road in the azimuthal angle for charged particles coming from the interaction region. The trigger required two charged particles, at least one of them tagged as an electron candidate by a signal from the corresponding Cherenkov section. Independently, two large energy depositions in the lead glass, separated by more than 90° in azimuth, were also required as a signature of the decay of a high mass object.

A preliminary event selection asked for compatibility of the two largest clusters in the calorimeter with the two charged tracks. A further cut was applied, calculating the invariant mass for the electron pair as $m_{ee}^2 = 2E_1E_2(1-\cos\theta_{12})$ (where E_1 and E_2 are the measured energies for the two largest clusters and θ_{12} is the opening angle between the corresponding tracks) and rejecting events with $m_{ee} < 2$ GeV/c^2.

The invariant mass (m_{ee}) distribution (fig. 4) shows the presence of a residual background dominated by Dalitz decays of the large π^0 component and by conversions of photons from π^0 decays, taking place predominantly in the 0.2 mm thick stainless steel vacuum pipe of the Accumulator ring. A signature for this background is an anomalously high signal from the scintillator counters (≈ 2 minimum ionizing particles equivalent) and a wide transverse shape of the electromagnetic shower in the lead glass.

To further improve on the J/ψ selection we therefore cut on three variables: the amplitude of the signal from the 4 mm thick scintillator layer (H2) and the two

Table 4
Average photoelectron yield for the small angle cell. The statistical errors are in the range of 0.5–1.5 pe

	1	2	3	4	5	6	7	8
$\langle n_{pe}\rangle$ $\theta < 24°$	14.6	16.3	15.7	14.7	13.1	14.0	14.5	13.8
(number of events)	(187)	(142)	(155)	(165)	(212)	(185)	(195)	(178)
$\langle n_{pe}\rangle$ $24° < \theta < 28°$	12.0	16.9	15.4	12.3	10.9	11.0	10.3	9.3
(number of events)	(132)	(175)	(176)	(136)	(154)	(121)	(154)	(145)
$\langle n_{pe}\rangle$ $28° < \theta < 32°$	8.2	17.3	10.3	8.1	7.5	7.0	7.1	6.3
(number of events)	(130)	(136)	(138)	(143)	(123)	(146)	(149)	(126)
$\langle n_{pe}\rangle$ $\theta > 32°$	3.6	6.8	5.2	4.3	4.0	2.2	6.1	5.8
(number of events)	(55)	(137)	(157)	(117)	(112)	(55)	(147)	(120)

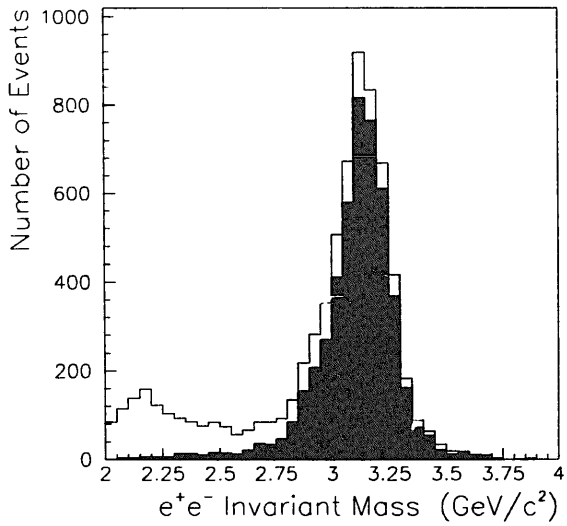

Fig. 4. Invariant mass distribution of final state e^+e^- pairs. The event selections are described in the text.

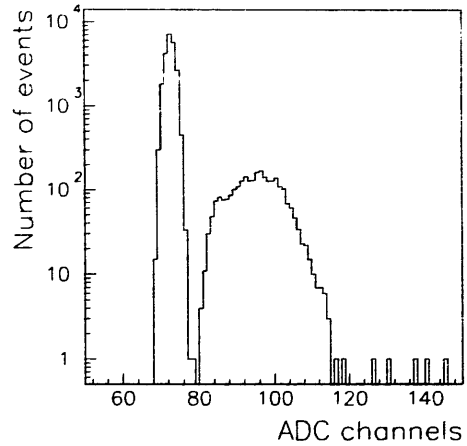

Fig. 5. Pedestal and thermal noise charge distribution (single photon) for one of the 16 PMs of the counter.

second transverse moments of the cluster energy. The final selection generated a clean J/ψ sample, as appears from the m_{ee} distribution (shaded in fig. 4).

4.2. Average number of photoelectrons

In tables 4 and 5 we summarize the measured average number of photoelectrons (pe) per electron, for each of the spherical and ellipsoidal mirrors. In order to measure the average number of photoelectrons per electron track, we use the Cherenkov signal pulse height distribution. The average pulse height can be converted to an average number of photoelectrons provided one knows the photomultiplier gain for the conditions of operation or, equivalently, the correspondence between ADC channels and number of photoelectrons leaving the photomultiplier's cathode. We achieve this by measuring the pedestal and the pulse height distribution of thermal noise for each PM (fig. 5); these measurements were frequently repeated during data taking. For the ellipsoidal mirrors, where path length in the radiator and image size depend strongly on the track polar angle, data are subdivided in four intervals of θ.

Typical distributions for a spherical and an ellipsoidal mirror are shown in figs. 6 and 7. The continuous lines represent normalized Poissonian fits, with the average number left as a free parameter. These fits give, in general, values that are close to the actual average reported in table 4, with the exception of mirrors 1 and 6 for $\theta > 32°$ where, however, the data are incompatible with a single Poissonian.

In fig. 8 the measured number of photoelectrons, averaged over the 8 mirrors in each cell, are compared to the simulation results; errors bars represent rms deviations of the individual mirror's averages.

From the number quoted in tables 4 and 5 we conclude that the mirror quality is uniform, except for two ellipsoidal mirrors (1 and 6 in table 4), where a lower number of photoelectrons is present at $\theta > 32°$

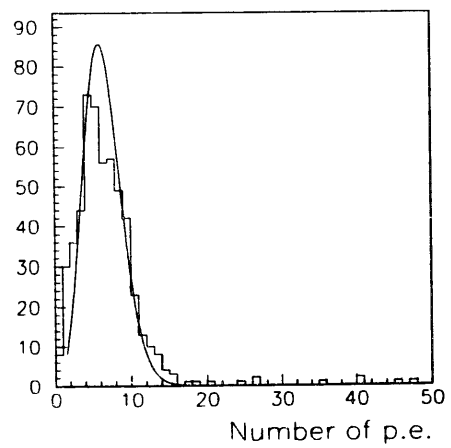

Fig. 6. Distribution of the number of photoelectrons for a typical spherical mirror.

Table 5
Average photoelectron yield for the large angle cell. The statistical errors are in the range of 0.5–1.5 pe

	1	2	3	4	5	6	7	8
$\langle n_{pe} \rangle$	8.0	6.1	9.7	6.9	7.0	8.9	7.3	9.8
Number of events	621	587	616	551	548	575	576	560

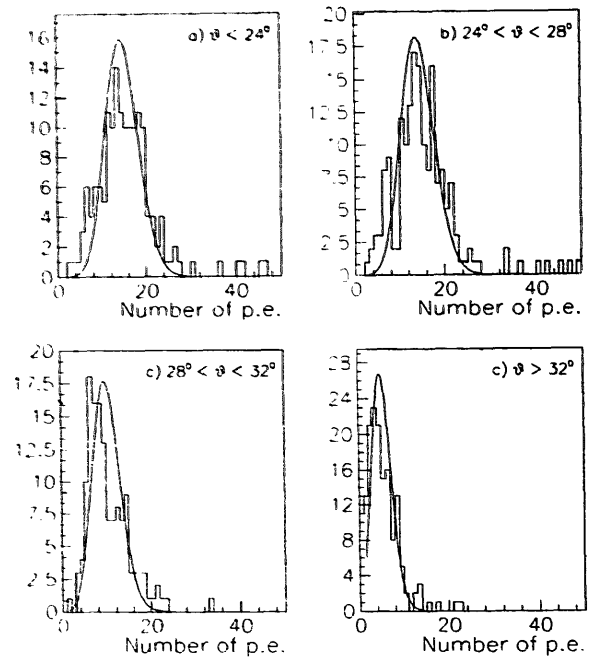

Fig. 7. Distribution of the number of photoelectrons for a typical ellipsoidal mirror for different intervals in θ angle: (a) $\theta < 24°$; (b) $24° < \theta < 28°$; (c) $28° < \theta < 32°$; (d) $\theta > 32°$.

as well as a lower number of events. This effect could be explained by a deformation of the mirror curvature in this region. This would lead to an enlargement of the image size on the PM window, with a corresponding loss in geometrical efficiency.

4.3. $e^{\pm}$ detection efficiency and $\pi^{\pm}$ rejection

In order to maximize electron detection efficiency, we set the Cherenkov discriminator threshold to a rather low value. With a threshold at 0.5 photoelectrons, the efficiency per electron, as measured over the angular range 15°–60° was (96.0 ± 0.4)% averaged over all sectors. The small loss is due almost entirely to the shadowing of the septum, and to the poor quality of two mirrors in the septum region. When the region $33° < \theta < 39°$ is not used, the efficiency is larger than 99.8%.

With such a low threshold, some contamination was to be expected, due both to the production of δ rays by hadron tracks in the gas radiator, and to baseline fluctuations in the PM signal. In order to measure this contamination, a clean sample of hadron tracks was obtained by selecting two-body final states with a trigger not requiring the Cherenkov signal. By kinematic constraints, we were able to separate the relatively weakly produced $\pi^+\pi^-$ from the dominant $p\bar{p}$ elastic. We have measured the photoelectron yield for pion and proton tracks: only about 1.2% of the pion tracks in the angular range 15°–60° could be associated with a signal above 0.5 photoelectrons; for protons, the corresponding fraction is quite similar. The low end of the PM pulse height distribution is compatible with baseline fluctuations. At a higher signal level (> 2 photoelectrons), the residual fraction is of the order of 0.7% for pions and 0.1% for protons, presumably originating from some physical source like δ rays.

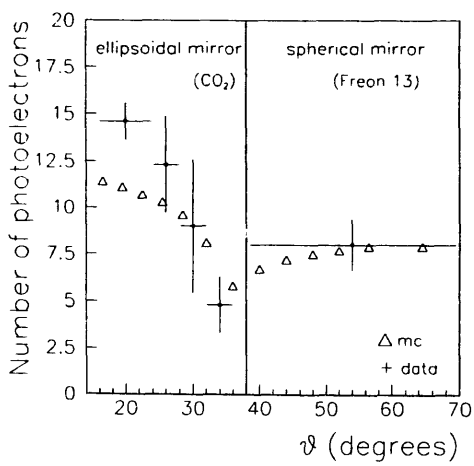

Fig. 8. Measured and calculated number of photoelectrons as a function of θ, averaged over ϕ.

Acknowledgements

We wish to thank all those who contributed to the success of this project. In particular P. Bomben and P. Fiocco, who developed the final technique to construct the carbon-fiber–epoxy panels; A. Braem and C. Nichols from CERN who, besides giving us valuable advice and decisive help in improving the surface quality of the carbon fiber mirrors, aluminized the plane glass mirrors and J. Penalver from CERN who undertook on a tight time schedule the large task of aluminizing all the other mirrors for us. Drs. J. Miller and C. Schuhl and many physicists and technicians of the LAL-Saclay gave us kind hospitality and effective help during early tests of a prototype counter. The effective help of Dr. S. Pordes and J. Sasek of the Fermi National Accelerator Laboratory during assembly of the counter is also gratefully acknowledged.

References

[1] T.A. Armstrong et al., Nucl. Phys. B373 (1992) 35.
[2] This technique was devised by P. Bomben and P. Fiocco, then at the Pianfei-IPA, Pianfei, Cuneo 12086, Italy.
[3] C. Biino et al., Nucl. Instr. and Meth. A239 (1985) 488.